HHS Public Access

Author manuscript

Adv Mater. Author manuscript; available in PMC 2018 May 01.

Published in final edited form as:

Adv Mater. 2017 May ; 29(17): . doi:10.1002/adma.201606129.

Ratiometric Photoacoustic Molecular Imaging for Methylmercury Detection in Living Subjects

Dr. Yi Liu,
School of Engineering, China Pharmaceutical University, Nanjing 210009, P. R. China. Laboratory of Molecular Imaging and Nanomedicine (LOMIN), National Institute of Biomedical Imaging and Bioengineering (NIBIB), National Institutes of Health (NIH), Bethesda, Maryland 20892, USA

Dr. Sheng Wang,
Guangdong Key Laboratory for Biomedical Measurements and Ultrasound Imaging, School of Biomedical Engineering, Shenzhen University, Shenzhen 518060, P. R. China. Key Laboratory of Optoelectronic Devices and Systems of Ministry of Education and Guangdong Province, College of Optoelectronic Engineering, Shenzhen University, Shenzhen 518060, P. R. China. Laboratory of Molecular Imaging and Nanomedicine (LOMIN), National Institute of Biomedical Imaging and Bioengineering (NIBIB), National Institutes of Health (NIH), Bethesda, Maryland 20892, USA

Dr. Ying Ma,
Laboratory of Molecular Imaging and Nanomedicine (LOMIN), National Institute of Biomedical Imaging and Bioengineering (NIBIB), National Institutes of Health (NIH), Bethesda, Maryland 20892, USA

Prof. Jing Lin,
Guangdong Key Laboratory for Biomedical Measurements and Ultrasound Imaging, School of Biomedical Engineering, Shenzhen University, Shenzhen 518060, P. R. China

Dr. Hai-Yan Wang,
Guangdong Key Laboratory for Biomedical Measurements and Ultrasound Imaging, School of Biomedical Engineering, Shenzhen University, Shenzhen 518060, P. R. China

Prof. Yueqing Gu,
School of Engineering, China Pharmaceutical University, Nanjing 210009, P. R. China

Prof. Xiaoyuan Chen, and
Laboratory of Molecular Imaging and Nanomedicine (LOMIN), National Institute of Biomedical Imaging and Bioengineering (NIBIB), National Institutes of Health (NIH), Bethesda, Maryland 20892, USA

Prof. Peng Huang
Guangdong Key Laboratory for Biomedical Measurements and Ultrasound Imaging, School of Biomedical Engineering, Shenzhen University, Shenzhen 518060, P. R. China

Correspondence to: Yueqing Gu; Xiaoyuan Chen; Peng Huang.

Supporting Information
Supporting Information is available from the Wiley Online Library or from the author.

Graphical Abstract

A promising $MeHg^+$ detection strategy by ratiometric photoacoustic molecular imaging shows very high sensitivity and selectivity in living subjects, such as zebrafish and mice.

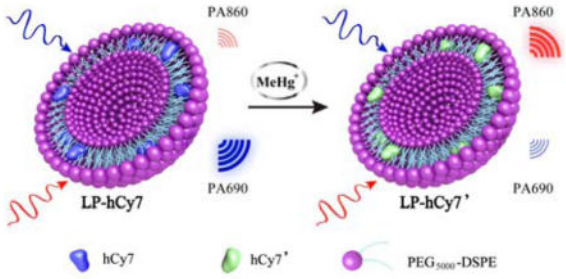

Keywords

Photoacoustic imaging; ratiometric probe; methylmercury detection; zebrafish

Photoacoustic imaging (PAI) is an emerging imaging modality based on the detection of ultrasonic wave generated by an optically excited chromophore.[1] With the development of photoacoustic (PA) contrast agents such as organic dyes,[2] carbon nanotubes[3] and metal-based nanoparticles,[4] PAI has been widely employed for tumor imaging,[5] therapeutic responses monitoring,[6] reactive oxygen species (ROS) detection,[7] pH detection,[8] enzyme detection,[9] metal ions detection,[10] and so on. The specificity and selectivity of PA contrast agents are the most crucial parts for the detection. To achieve analyte-specific PA detection, the recognition site of PA detector should be activated by the specific analyte, and followed by an obvious change of PA signal intensity with high sensitivity. For metal ion detection, Chan *et al.* developed a PA detector with a 2-picolinic ester sensing module that is readily hydrolyzed in the presence of copper (Cu^{2+}) for the chemoselective visualization of Cu^{2+}, which is a crucial metal ion in chronic nervous diseases (e.g. Alzheimer's disease).[10a] In another case, Clark *et al.*[10b] reported that a PA sensor composed of a lithium (Li^+) selective crown ether ionophore, lithium ionophore VI (L) and a chromoionophore (CH^+) is selected for *in vivo* measurement of Li^+ concentrations. Li^+ is recognized and extracted into the hydrophobic polymer core of the sensor, leading to the deprotonation of chromoionophore, which changes the PA signal intensity of the sensor. Therefore, the development of novel PA detectors for other metal ions is highly desirable.

Methylmercury ($MeHg^+$) readily accumulates in the food chain, such as fish. It is one of the most potent neurotoxins, which damages the brain and nervous systems of human beings through fish consumption, especially for pregnant women and infants. Currently, the $MeHg^+$ detection methods mainly include gas chromatography (GC), high-performance liquid chromatography (HPLC) or capillary electrophoresis (CE) coupled to a specific detector such as atomic fluorescence spectrometry (AFS), mass spectrometry (MS), or inductively coupled plasma mass spectrometry (ICP-MS).[11] Additionally, the pre-treatment of samples is also rather complicated. Therefore, there is a high demand for a simple, robust, real-time

and visual method for *in vivo* detection and monitoring of $MeHg^+$, especially for living fishes.

Herein, we report a chemoselective PA sensor (LP-hCy7) composed of the liposome (LP) and $MeHg^+$-responsible near-infrared (NIR) cyanine dye (hCy7)[12] for $MeHg^+$ detection within a living subjects (Scheme 1). In the LP-hCy7 nanoprobe, the hydrophobic hCy7 was encapsulated in the lipid layer of liposome. When the LP-hCy7 was treated with $MeHg^+$, the strong liposoluble $MeHg^+$ easily went into the lipid layer of LP-hCy7, thus converting hCy7 into hCy7' through mercury-promoted cyclization reaction. The absorbance intensities of nanoprobes at 690 and 860 nm would be decreased and increased, respectively. It also led to the increase of ratiometric photoacoustic signal (PA860/PA690) in the presence of $MeHg^+$. Importantly, using PA860/PA690 as an indicator, LP-hCy7 allows to monitor the concentration of $MeHg^+$ by ratiometric photoacoustic bioimaging in living subjects.

Firstly, we synthesized hCy7 *via* coupling reaction between hNIR-Cl and thiosemicarbazide subunit (Scheme S1, Figure S1–3 Supporting information).[12] Then the hydrophobic hCy7 was encapsulated into the lipid layer of liposome to achieve a chemoselective nanoprobe (LP-hCy7) for $MeHg^+$ detection.[13] The morphology and size of the LP-hCy7 were characterized by transmission electron microscopy (TEM) and dynamic light scattering (DLS), respectively. As shown in Figure 1a, the LP-hCy7 was well dispersed with an average diameter of ~50 nm. The hydrodynamic diameter of LP-hCy7 was 98.2 ± 22.4 nm (Figure 1b). Fourier transform infrared spectroscopy (FTIR) spectra and ^1H NMR spectra further demonstrated that the organic dye hCy7 molecules were successfully doped in the liposomes (Figure S4 and S5, Supporting information). To examine the optical response of the nanoprobe LP-hCy7 to $MeHg^+$ ions, the absorption spectra of LP-hCy7 with different concentrations of $MeHg^+$ were measured by using UV-vis-NIR spectrophotometer. As shown in Figure 1c, upon addition of MeHgCl, the optical density (OD) of LP-hCy7 at 690 nm (OD690) decreased gradually. Meanwhile, the OD at 860 nm (OD860) gradually increased with the increasing amount of MeHgCl. The colour of the LP-hCy7 solution with the addition of $MeHg^+$ changed obviously from blue to weak green (Figure 1d). These results indicated that the hCy7 in the hydrophobic layer of LP-hCy7 reacted with $MeHg^+$, leading to the structure change from hCy7 to hCy7'. The responsive mechanism of the reaction of LP-hCy7 with $MeHg^+$ was confirmed by liqiud chromatography-mass spectrometry (LC-MS). The peak at m/z 1194.8 (calculated as 1194.8) was ascribed to hCy7, and the peak at m/z 1160.8 (calculated as 1160.8) was assigned to hCy7' (Figure S6, Supporting information).[14] Moreover, the time-dependent absorbance spectra of LP-hCy7 with different amounts of $MeHg^+$ ions also gave a significant change of OD (Figure S7, Supporting information).

It is no surprise that the photoacoustic signal of hCy7 would also change with the interaction between hCy7 and $MeHg^+$. As shown in Figure 2a, the LP-hCy7 has a high photoacoustic signal at 690 nm (PA690) and a low photoacoustic signal at 860 nm (PA860), resulting in a very low PA860/PA690 value (~0.06). However, in the presence of $MeHg^+$, the PA860 of LP-hCy7' increased. At the same time, PA690 of LP-hCy7' was lower than that of LP-hCy7 due to reduced absorbance at 690 nm. Therefore, the PA860/PA690 of LP-hCy7'was significantly increased, with a value of about 1.0, which is about 16-fold higher than that of

LP-hCy7 (Figure 2c). Furthermore, a linear relationship between the PA860/PA690 and $MeHg^+$ concentration in the range of 0–5 μM (Figure 2b) was observed, and the detection limit of nanoprobe LP-hCy7 for $MeHg^+$ in aqueous solution was measured to be 2.0 ppb, which is comparable to that of UV-vis-NIR spectrophotometer method (Figure S8, Supporting information). The time-dependent PA860/PA690 of LP-hCy7 with different amounts of $MeHg^+$ ions also gave a ratio increase of PA860/PA690 with time (Figure S9, Supporting information).

Next, the specificity and selectivity of nanoprobe LP-hCy7 were investigated. Significantly, the photoacoustic response of LP-hCy7 nanoprobe toward $MeHg^+$ relative to some other metal ions, including some alkaline earth (Ca^{2+}, Mg^{2+}), and transition-metal ions (Mn^{2+}, Fe^{2+}, Co^{2+}, Ni^{2+}, Zn^{2+}, Cu^{2+}), were detected under the same condition. The results revealed that only the addition of $MeHg^+$ induced a prominent change in both absorbance spectra and photoacoustic imaging, while negligible change was caused by adding excessive other metal ions (Figure 2c; Figure S10, (Supporting information)). Taken together, these results indicated that the LP-hCy7 nanoprobe can serve as a colorimetric and photoacoustic chemodosimeter for the detection of $MeHg^+$ with high sensitivity and selectivity.

The cytotoxicity and biocompatibility of LP-hCy7 nanoprobes were investigated on U87MG cells by using the methyl thiazolyl tetrazolium (MTT) assay. After the cells were incubated with LP-hCy7 (0–500 μg/mL) for 24 h, no significant change in the proliferation of cells was observed (Figure S11, Supporting information). Even at 500 μg/mL of LP-hCy7, the cellular viability of cells was still over 85%, indicating the negligible toxicity of LP-hCy7 nanoprobes.

Encouraged by the photoacoustic and biological properties of LP-hCy7 nanoprobes, we investigated the potential of LP-hCy7 as a ratiometric photoacoustic detector for real-time monitoring of $MeHg^+$ level *in vivo* using zebrafish model.[15] As a proof of concept experiment, zebrafishes with/without contamination of $MeHg^+$ were incubated with LP-hCy7 (0.1 mg/mL). The zebrafishes without any treatment were used as control. Then all zebrafishes were detected by PAI.

We used the 3D ultrasonic imaging to identify the location of zebrafishes (Figure 3a). The photoacoustic images in transection of abdomen of zebrafishes at wavelength of both 690 and 860 nm were recorded in Figure 3b1–b9. The photoacoustic intensities were measured in Figure 3c. The untreated zebrafishes in the control group have no obvious photoacoustic signals at 690 nm (PA690) and 860 nm (PA860). For LP-hCy7 incubated zebrafishes without contamination of $MeHg^+$, they exhibited strong PA690 and weak PA860 with a PA860/PA690 value of about 0.27 (Figure 3d). For LP-hCy7 incubated zebrafishes with contamination of $MeHg^+$, the PA690 decreased obviously and the PA860 increased with PA860/PA690 up to 2.82 (Figure 3d). Normalization of the PA ratios resulted in a ratiometric photoacoustic turn-on of 10.44-fold after $MeHg^+$ incubation.

We also tested this method in living mice. The photoacoustic images of subcutaneous tissues of mice at both 690 and 860 nm were recorded in Figure S12a. The photoacoustic intensities were measured in Figure S12b, the control group had no obvious photoacoustic signals at

690 nm (PA690) and 860 nm (PA860). However, the LP-hCy7 treated mice exhibited strong PA690 and weak PA860 with a PA860/PA690 value of about 0.11 (Figure S12c). With pre-injection of $MeHg^+$, it can be found that the PA690 decreased obviously and the PA860 increased with PA860/PA690 up to 1.97 (Figure S12c). Normalization of the PA ratios resulted in a ratiometric photoacoustic turn-on of 17.9-fold after $MeHg^+$ involvement. These above findings indicate that the LP-hCy7 nanoprobe could effectively detect $MeHg^+$ in living subjects, such as zebrafish and mice, through ratiometric photoacoustic imaging.

In summary, we have developed a turn-on ratiometric photoacoustic LP-hCy7 nanoprobe for $MeHg^+$ PA detection *in vitro* and *in vivo*. LP-hCy7 displayed unique dual-shift NIR absorbance peaks and produced a normalized turn-on response after $MeHg^+$ incubation. More importantly, the LP-hCy7 nanoprobe was shown to be capable of monitoring $MeHg^+$ *in vivo* by ratiometric photoacoustic bioimaging. These findings not only provided a ratiometric photoacoustic molecular imaging for *in vivo* metal ions detection but also opened the door of a new imaging technique as “spectroscopic photoacoustic molecular imaging” for biomedical applications.

Supplementary Material

Refer to Web version on PubMed Central for supplementary material.

Acknowledgments

Y. L and S. W. contributed equally to this work. The authors thank the National Science Foundation of China (51573096, 81601531, 81401465), National Science Foundation of Jiangsu Province (BK20160755) and the Intramural Research Programs of the National Institute of Biomedical Imaging and Bioengineering (NIBIB), National Institutes of Health (NIH).

References

1. a) Wang LV. Nat Photonics. 2009; 3:503. [PubMed: 20161535] b) Xia J, Yao J, Wang LV. Electromagn Waves. 2014; 147:1.c) Nie L, Chen X. Chem Soc Rev. 2014; 43:7132. [PubMed: 24967718] d) Liu Y, Nie L, Chen X. Trends Biotech. 2016; 34:420.e) Wang S, Lin J, Wang T, Chen X, Huang P. Theranostics. 2016; 6:2394. [PubMed: 27877243] f) Lin J, Chen X, Huang P. Adv Drug Deliver Rev. 2016; 105:242.
2. a) Huang P, Rong P, Jin A, Yan X, Zhang MG, Lin J, Hu H, Wang Z, Yue X, Li W. Adv Mater. 2014; 26:6401. [PubMed: 25123089] b) Lovell JF, Jin CS, Huynh E, Jin H, Kim C, Rubinstein JL, Chan WC, Cao W, Wang LV, Zheng G. Nat Mater. 2011; 10:324. [PubMed: 21423187] c) Huynh E, Leung BY, Helfield BL, Shakiba M, Gandier JA, Jin CS, Master ER, Wilson BC, Goertz DE, Zheng G. Nat Nanotech. 2015; 10:325.d) Li LL, Ma HL, Qi GB, Zhang D, Yu F, Hu Z, Wang H. Adv Mater. 2016; 28:254. [PubMed: 26568542] e) Zhang D, Qi GB, Zhao YX, Qiao SL, Yang C, Wang H. Adv Mater. 2015; 27:6125. [PubMed: 26350172]
3. a) De La Zerda A, Zavaleta C, Keren S, Vaithilingam S, Bodapati S, Liu Z, Levi J, Smith BR, Ma TJ, Oralkan O. Nat Nanotech. 2008; 3:557.b) Zerda, Adl, Liu, Z., Bodapati, S., Teed, R., Vaithilingam, S., Khuri-Yakub, BT., Chen, X., Dai, H., Gambhir, SS. Nano Lett. 2010; 10:2168. [PubMed: 20499887]
4. a) Eghtedari M, Oraevsky A, Copland JA, Kotov NA, Conjusteau A, Motamedi M. Nano Lett. 2007; 7:1914. [PubMed: 17570730] b) Kim JW, Galanzha EI, Shashkov EV, Moon HM, Zharov VP. Nat Nanotech. 2009; 4:688.c) Xia Y, Li W, Cobley CM, Chen J, Xia X, Zhang Q, Yang M, Cho EC, Brown PK. Acc Chem Res. 2011; 44:914. [PubMed: 21528889] d) Jokerst JV, Cole AJ, Van de Sompel D, Gambhir SS. ACS Nano. 2012; 6:10366. [PubMed: 23101432] e) Huang P, Lin J, Li W, Rong P, Wang Z, Wang S, Wang X, Sun X, Aronova M, Niu G. Angew Chem Int Ed. 2013;

125:14208.f) Cheng L, Liu J, Gu X, Gong H, Shi X, Liu T, Wang C, Wang X, Liu G, Xing H. Adv Mater. 2014; 26:1886. [PubMed: 24375758] g) Liang S, Li C, Zhang C, Chen Y, Xu L, Bao C, Wang X. Theranostics. 2015; 5:970. [PubMed: 26155313] h) Bao C, Conde J, Pan F, Li C, Zhang C, Tian F, Liang S, Jesus M, Cui D. Nano Res. 2016; 9:1043.

5. a) Fan Q, Cheng K, Yang Z, Zhang R, Yang M, Hu X, Ma X, Bu L, Lu X, Xiong X. Adv Mater. 2015; 27:843. [PubMed: 25376906] b) Lin J, Wang M, Hu H, Yang X, Wen B, Wang Z, Jacobson O, Song J, Zhang G, Niu G, Huang P, Chen X. Adv Mater. 2016; 28:3273. [PubMed: 26928972] c) Wang Z, Huang P, Jacobson O, Wang Z, Lu N, Zhang H, Lin J, Niu G, Liu G, Chen X. ACS Nano. 2016; 10:3453. [PubMed: 26871955] d) Huang P, Gao Y, Lin J, Hu H, Liao H, Yan X, Tang Y, Jin A, Song J, Niu G, Zhang G, Horkay F, Chen X. ACS Nano. 2015; 9:9517. [PubMed: 26301492]
6. Nie L, Huang P, Li W, Yan X, Jin A, Wang Z, Tang Y, Wang S, Zhang X, Niu G, Chen X. ACS Nano. 2014; 8:12141. [PubMed: 25406986]
7. Pu K, Shuhendler AJ, Jokerst JV, Mei J, Gambhir SS, Bao Z, Rao J. Nat Nanotechnol. 2014; 9:233. [PubMed: 24463363]
8. a) Chen Q, Liu X, Chen J, Zeng J, Cheng Z, Liu Z. Adv Mater. 2015; 27:6820. [PubMed: 26418312] b) Miao Q, Lyu Y, Ding D, Pu K. Adv Mater. 2016; 28:3662. [PubMed: 27000431]
9. Yang K, Zhu L, Nie L, Sun X, Cheng L, Wu C, Niu G, Chen X, Liu Z. Theranostics. 2014; 4:134. [PubMed: 24465271]
10. a) Li H, Zhang P, Smaga LP, Hoffman RA, Chan J. J Am Chem Soc. 2015; 137:15628. [PubMed: 26652006] b) Cash KJ, Li C, Xia J, Wang LV, Clark HA. ACS Nano. 2015; 9:1692. [PubMed: 25588028]
11. Ding Y, Wang S, Li J, Chen L. TrAC, Trends Anal Chem. 2016; 82:175.
12. a) Liu Y, Chen M, Cao T, Sun Y, Li C, Liu Q, Yang T, Yao L, Feng W, Li F. J Am Chem Soc. 2013; 135:9869. [PubMed: 23763640] b) Yang Y, Zhao Q, Feng W, Li F. Chem Rev. 2013; 113:192. [PubMed: 22702347] c) Feng W, Han C, Li F. Adv Mater. 2013; 25:5287. [PubMed: 23982981]
13. Wang S, Zhang S, Liu J, Liu Z, Su L, Wang H, Chang J. ACS Appl Mater Interfaces. 2014; 6:10706. [PubMed: 24941446]
14. Guo Z, Zhu W, Zhu M, Wu X, Tian H. Chem-Eur J. 2010; 16:14424. [PubMed: 21038328]
15. Peng J, Xu W, Teoh CL, Han S, Kim B, Samanta A, Er JC, Wang L, Yuan L, Liu X. J Am Chem Soc. 2015; 137:2336. [PubMed: 25626163]

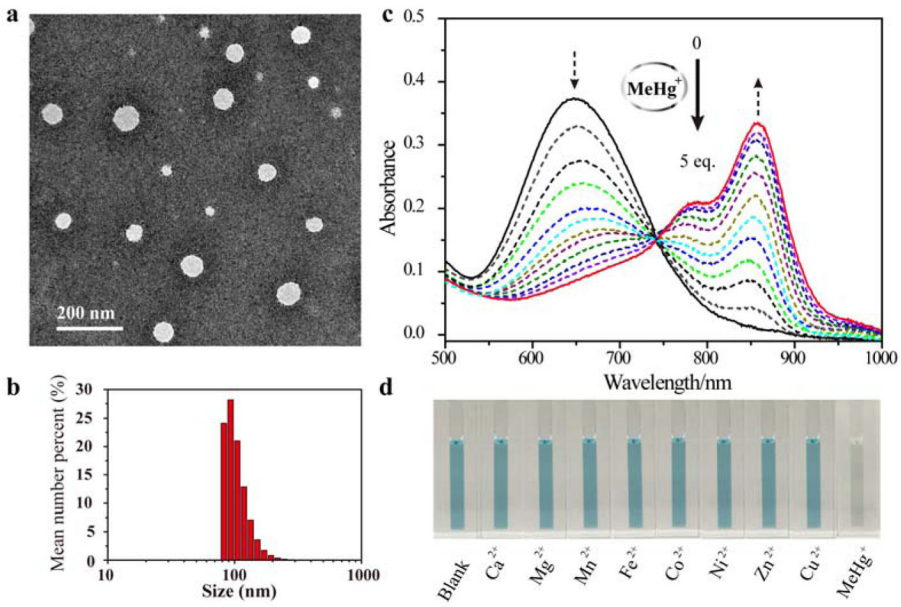

Figure 1.

a) TEM image of nanoprobe LP-hCy7. b) DLS result of LP-hCy7. c) Absorbance response of LP-hCy7 as a function of $MeHg^{+}$ concentration (0–20 μM) in an aqueous solution. d) Photographs showing the colour changes of the aqueous solution of LP-hCy7 in the presence of various representative metal ions (Ca^{2+}, Mg^{2+}, Mn^{2+},Fe^{2+}, Co^{2+}, Ni^{2+}, Zn^{2+}, Cu^{2+} and $MeHg^{+}$).

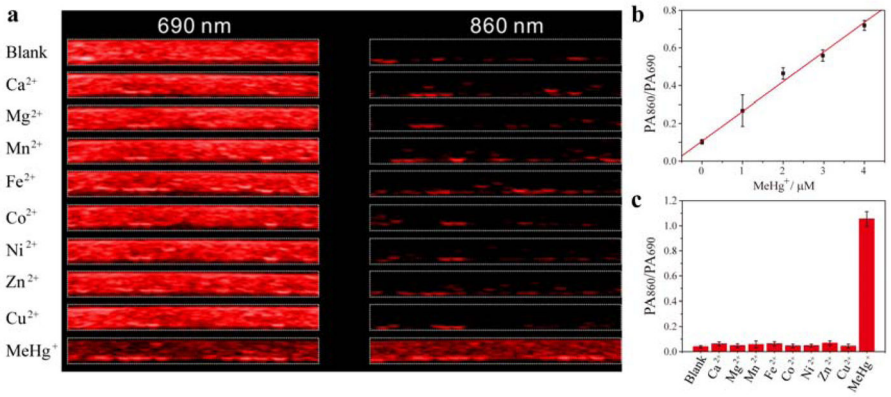

Figure 2.

a) *In vitro* PA images of the aqueous solution of LP-hCy7 in the presence of various representative metal ions (Ca^{2+}, Mg^{2+}, Mn^{2+}, Fe^{2+}, Co^{2+}, Ni^{2+}, Zn^{2+}, Cu^{2+} and $MeHg^{+}$) at 690 (left) and 860 nm (right), respectively. b) Polt of the PA860/PA690 of LP-hCy7 against the concentration of $MeHg^{+}$ ions. c) PA860/PA690 of the LP-hCy7 in the presence of various representative metal cations.

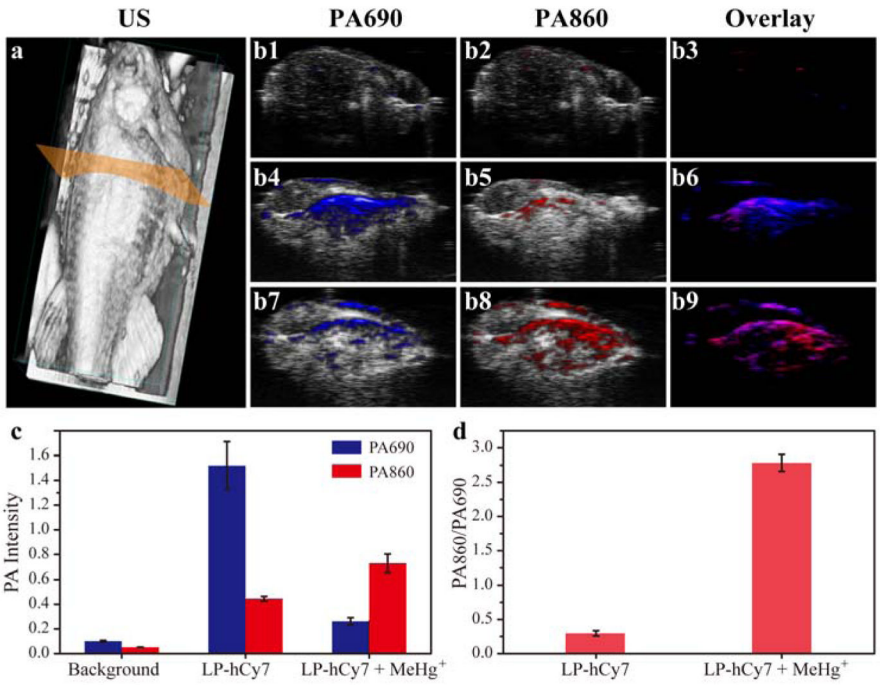

Figure 3.

a) 3D ultrasonic (US) image of zebrafish for illustration of photoacoustic imaging in transection of abdomen. b) merged US and PA images of untreated zebrafish (b1-b3), LP-hCy7 incubated zebrafish (b4-b6) and $MeHg^{+}$/LP-hCy7 treated zebrafish (b7-b9) at 690 (left) and 860 nm (right), respectively. c) Corresponding quantified PA intensity at 690 nm (blue) and 860 nm (red) for b. d) Ratios of PA860/PA690 obtained from b. (n = 4/group)

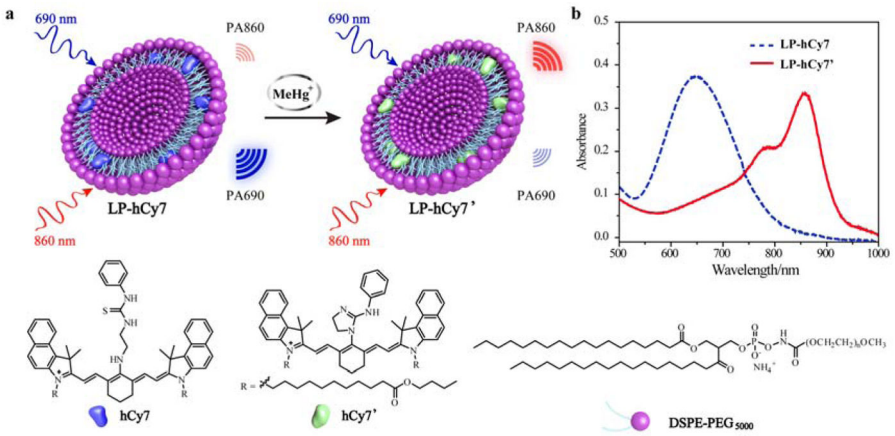

Scheme 1.

a) Schematic illustration of proposed strategy for ratiometric photoacoustic imaging of $MeHg^+$. b) Absorbance spectra of LP-hCy7 in absence (blue) and presence (LP-hCy7', red) of $MeHg^+$.